Using parabolized stability equations to model boundary-layer transition in direct and large-eddy simulations

A. Lozano-Durán*, M. J. P. Hack [†], and P. Moin [‡]
Stanford University, Stanford, CA, 94305

We examine the potential of the nonlinear parabolized stability equations (PSE) to provide an accurate yet computationally efficient treatment of the growth of disturbances in H-type transition to turbulence. The PSE capture the nonlinear interactions that eventually induce breakdown to turbulence, and can as such identify the onset of transition without relying on empirical correlations. Since the local PSE solution at the onset of transition is a close approximation of the Navier-Stokes equations, it provides a natural inflow condition for direct numerical simulations (DNS) and large-eddy simulations (LES) by avoiding nonphysical transients. We show that a combined PSE/DNS approach, where the pre-transitional region is modeled by the PSE, can reproduce the skin-friction distribution and downstream turbulent statistics from a DNS of the full domain.

I. Introduction

Modeling the laminar-turbulent transition remains one of the key challenges in the numerical simulation of boundary layers, especially at coarse grid resolutions. The issue is particularly relevant in wall-modeled large-eddy simulations (LES), which require 10 to 100 times more grid points in the thin laminar region than in the turbulent regime to properly capture the instabilities preceding the transition [1]. Our study examines the potential of the nonlinear parabolized stability equations (PSE) to provide an accurate yet computationally efficient treatment of the disturbances in the pre-transitional zone. An extended version of the present work can be found in Lozano-Durán et al. [2].

Direct numerical simulation (DNS) of the Navier-Stokes equations has been frequently used as a tool to investigate transitional flows. However, its computational cost is unaffordable in most practical settings. In order to explore more computationally efficient approaches, [3] conducted LES of K- and H-type transitional boundary layers. They found that constant coefficient models for the subgrid-scale stress tensor could not predict the rapid rise in skin friction at the onset of transition. The reasons were traced back to the non-negligible turbulent viscosity in the laminar region, which dampens the amplification of instabilities. Dynamic models sufficiently reduced the turbulent viscosity in the laminar flow and allowed the growth of disturbances. When the grid was fine enough, LES reproduced the skin-friction overshoot observed in DNS. However, the calculations above do not exploit the flow structure during the pre-transitional stages and still require a relatively large number of grid points to capture the growth of instabilities in this region.

The PSE have opened new avenues to the analysis of the spatial growth of linear and nonlinear disturbances in slowly varying shear flows such as boundary layers, jets, and far wakes. The approach captures nonparallel effects as well as nonlinear interactions between modes that eventually induce breakdown to turbulence. This allows to identify the onset of transition without relying on empirical correlations in contrast to Reynolds-averaged Navier-Stokes (RANS) equations models [e.g., 4].

The present study aims to combine the individual advantages of PSE and LES to enable the accurate and efficient simulation of transitional boundary layers. In the laminar regime, the streamwise evolution of the instability waves is captured using the nonlinear form of PSE. Once the flow begins to transition, the local PSE solution is used as the inflow boundary condition in a direct or large-eddy simulation. Since the local PSE solution in the pre-transitional boundary layer is a close approximation of the solution of the Navier-Stokes equations, it is expected to provide a natural inflow condition for both LES and DNS by avoiding nonphysical transients.

We show that in a classic H-type transition scenario, a combined PSE-DNS and PSE-LES approach predicts the point of transition and reproduce the correct physical behavior in both the pre-transitional and turbulent regions. When compared to simulations where DNS or LES are used for the entire domain, the computational cost is reduced by several orders of magnitude.

---

*Post-doctoral fellow, Center for Turbulence Research, Stanford University. Member AIAA
[†]Post-doctoral fellow, Center for Turbulence Research, Stanford University. Member AIAA
[‡]Franklin P. and Caroline M. Johnson Professor, Department of Mechanical Engineering, Stanford University. Fellow AIAA

II. Parabolized stability equations for modeling the pre-transitional region

Since first proposed by Herbert [5] and Bertolotti et al. [6], the PSE have become a well-established method for the study of disturbance growth up to the breakdown stage, where significant changes in the skin friction occur. Different formulations can be found in the literature [7], and in the present work we adopt the nonlinear PSE from Hack and Moin [8]. In this case, frequencies and wavenumbers are solved simultaneously to trace the nonlinear evolution of single modes and the interaction of different ones. Comparisons of linear and nonlinear PSE are reported by Esfahanian et al. [9].

We outline below the key components of the PSE methodology. For a detailed description the reader is referred to Lozano-Durán et al. [2], and previous works by Hack and Moin [8], Herbert [5] and Bertolotti et al. [6]. Let us consider a flat-plate transitional boundary layer. In the following, the streamwise, wall-normal and spanwise directions are denoted by x, y, and z, respectively, and the corresponding velocity components by u, v, and w, or in vector form by $\boldsymbol{u}$. The PSE exploit the fact that, during the pre-transitional stage, the velocities can be rearranged as the product of fast and slowly changing components in x that will be later used to further simplify the equations. For the streamwise velocity

$$u(x,y,z) = U(x,y) + \sum_n^N \sum_m^M \widehat{u}_{n,m}^{\text{slow}}(x,y) e^{in\beta z - im\omega t} e^{i\theta_{n,m}(x)}, \tag{1}$$

where U is the base flow (or Blasius solution in this particular case), N and M are the total number of spanwise and temporal Fourier modes, $n\beta$ and $m\omega$ their respective wavenumbers, and $e^{i\theta_{n,m}(x)}$ and $\widehat{u}_{n,m}^{\text{slow}}(x,y)$ the fast and slowly changing components. Similar expressions apply to v and w. This decomposition is not uniquely defined and an extra constraint has to be specified in order to remove the ambiguity. One reasonable option often used in the literature is to impose constant average-fluctuating kinetic energy of the slowly changing velocity on x

$$\frac{\partial}{\partial x} \int_0^\infty \frac{1}{2} |\widehat{\boldsymbol{u}}_{n,m}^{slow}|^2 \mathrm{d}y = 0, \tag{2}$$

although other normalization conditions are possible and have been shown to produce similar results [10–12].

Introducing Eq. (1) into the Navier-Stokes equations provides a system that is still exact in the limit of infinite Fourier series. The advantages with respect to the usual formulation are obtained by retaining terms up to $\mathcal{O}(Re^{-1})$ and by a strong truncation in the number of spanwise and temporal modes. This simplifies the set of equations and defines the usual nonlinear PSE that can be solved at a modest computational expense. Besides the reduced number of Fourier modes, the slow streamwise variation of the velocities allows for larger grid spacing in the mean flow direction, and the implementation of a marching procedure scheme in the streamwise direction further simplifies the problem by neglecting the remaining non-parabolic nature of the equations in x [11]. The combined effect of all previous factors results in substantial computational savings. The marching procedure terminates when the iterative update of the wavenumber or solution of the nonlinear system fails to converge. This is typically related to the rapid growth of nonlinear effects and the limited length of the Fourier series that produce an inaccurate representation of the flow.

III. Numerical experiments

We perform three numerical simulations. The setup is a zero-pressure-gradient flat-plate boundary layer from laminar to turbulent flow through H-type natural transition [5]. Unless otherwise stated, velocities are non-dimensionalized by the free-stream streamwise velocity U_∞. Wall units are denoted by superscript + and defined in terms of u_τ, ν, and δ, where $u_\tau \equiv \sqrt{\nu \frac{\partial U}{\partial y}|_{y=0}}$ is the friction velocity, ν is the kinematic viscosity of the flow, and δ is the boundary thickness at 99% of U_∞. We define δ_0 as δ at the inlet location. The Reynolds number based on the distance to the leading edge and momentum thickness are Re_x and Re_θ, respectively.

Transition is triggered by imposing an inflow condition consisting of the Blasius solution plus disturbances obtained from the linear Orr-Sommerfeld/Squire problem. In particular, we prescribe the disturbance in terms of a fundamental Tollmien-Schlichting (TS) wave and a subharmonic oblique wave at $Re_x = 1.8 \times 10^5$. The fundamental non-dimensional frequency of the TS wave is $F = \omega\nu/U_\infty^2 = 1.2395 \times 10^{-4}$. The subharmonic frequency is set to $F/2$. Following [10], the amplitudes of the fundamental and subharmonic disturbances are 0.0048 and 0.145×10^{-4}, respectively, and the spanwise wavenumber of the latter is $\beta\delta_0 = 0.6888$. Regarding the remaining boundary conditions, the Blasius solution is used at the top of the computational domain and convective outflow at the outlet. The spanwise direction is periodic.
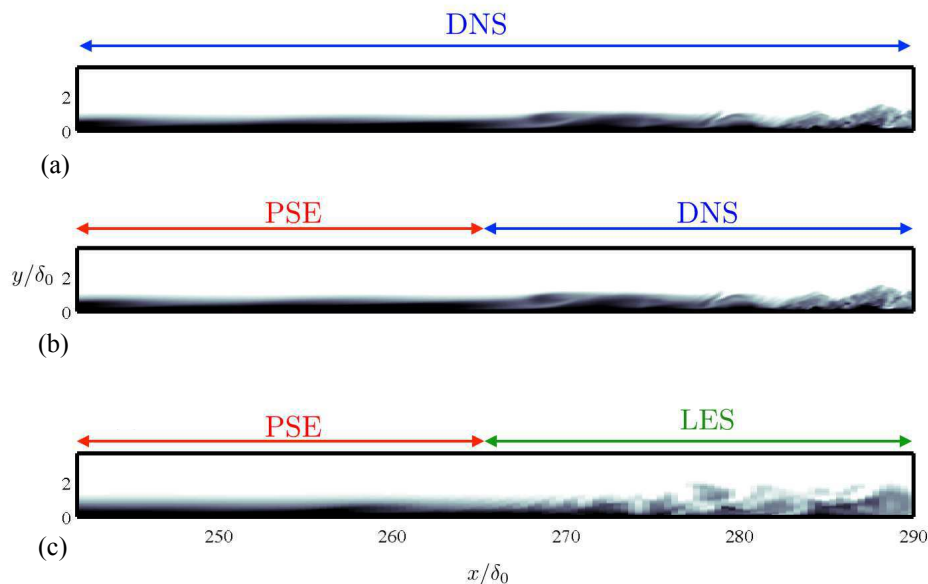
2

Fig. 1 Sketches of zero-pressure-gradient flat-plate transitional boundary layers for the three cases under consideration. Colors represent streamwise velocity from zero (black) to free-stream velocity (white). The arrows delimit the regions where different methodologies are used to compute the flow solution. (a) DNS-DNS case, (b) PSE-DNS case, and (c) PSE-LES case. Note that the domains are not to scale and the actual details of the simulations are summarized in Table 1. The exact matching location between PSE and DNS/LES is at $Re_x = 4.0 \times 10^5$.

The length, height and width of the simulated box are $L_x = 305\delta_0$, $L_y = 30\delta_0$ and $L_z = 20\delta_0$. All computations were run for 10 periods of the fundamental frequency (after transients) with 100 velocity fields stored per period and equally spaced in time.

We will investigate the potential of PSE for modeling the pre-transitional region through three numerical experiments named DNS-DNS, PSE-DNS and PSE-LES. In each experiment, the pre-transitional zone is computed using either PSE or DNS (with the same inflow condition described above), and the transitional and turbulence region with DNS or LES. The domain decomposition of each experiment is sketched in Fig. 1 and their corresponding parameters are summarized in Table 1. The matching location between PSE and DNS/LES is set at $Re_x = 4.0 \times 10^5$. Preliminary studies showed the necessity of a fully consistent DNS case where the inflow conditions are identical to those used for PSE calculations in order to make meaningful comparisons. Therefore, DNS-DNS is used as the reference case. PSE-DNS will assess the suitability of PSE for treating the pre-transitional region. In the last case, PSE-LES, we will explore further computational savings by combining PSE for the pre-transitional region, and LES for the transitional and turbulent zones as expected to be required for most engineering applications.

DNS and LES solutions are computed by integrating the incompressible Navier-Stokes equations with staggered second-order central finite differences approximations [13]. Time advancement is achieved by a third-order Runge-Kutta scheme [14], combined with the fractional-step procedure [15]. LES calculations are carried out with the dynamic Smagorinsky subgrid-scale model as in Germano et al. [16] and Lilly [17] but without averaging in the homogeneous direction. The code is parallelized using message passing interface with a global transpose from y-z to x-y planes and has been validated in previous investigations [18–20]. The numerical approach for solving PSE can be found in Hack and Moin [8]. Seven modes were used for solving the PSE in all of the cases. Given the streamwise parabolic nature of the discretized PSE, the coupling between PSE and DNS/LES is effectively imposed as an inflow boundary condition in the latter.

As an example, Fig. 2 shows the emergence of the characteristic staggered configuration of lambda vortices from DNS-DNS.

3

	Pre-transition				Transition+turbulence				
Case	Δx^+	Δy^+_{min}	Δz^+	N_{points}	Δx^+	Δy^+_{min}	Δz^+	N_{points}	N_{total}
DNS-DNS	7.2	0.3	5.1	100M	7.2	0.3	5.1	150M	250M
PSE-DNS	44.0	0.2	-	0.2M	7.2	0.3	5.1	150M	150.2M
PSE-LES	44.0	0.2	-	0.2M	45.0	1.0	22.0	4M	4.2M

Table 1   Parameters of the three different numerical experiments. Δx and Δz **are the streamwise and spanwise grid spacing, and** Δy_{min} **is the minimum (closest to the wall) wall-normal resolution. For PSE, seven spanwise Fourier modes are used.** N_{points} **is the number of million grid points for each particular region and case, and** N_{total} **is the total number of points in the full domain.**
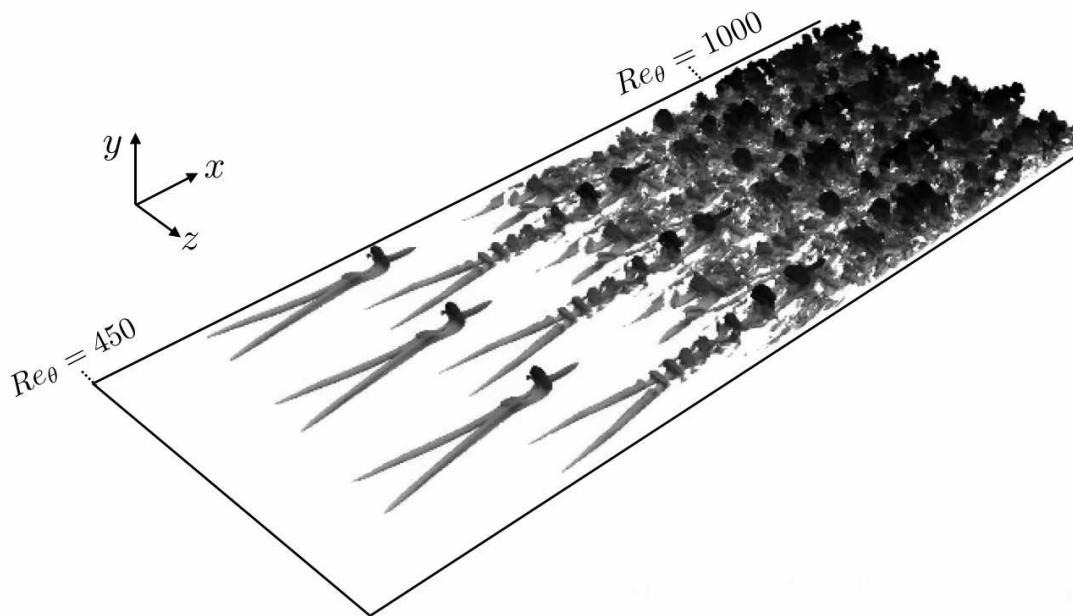

Fig. 2   Isocontours of positive instantaneous wall-normal velocity at a value of $3 \times 10^{-2} U_\infty$ **for DNS-DNS.**
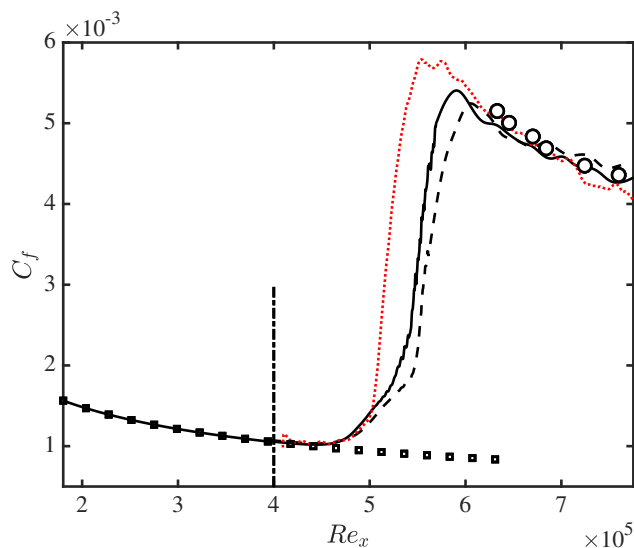
4

Fig. 3   Skin-friction coefficient as a function of the Reynolds number. Solid black line, DNS-DNS; dashed black line, PSE-DNS; dotted red line, PSE-LES; black squares, Blasius correlation; black circles circles, correlation from the DNS by Sayadi et al. [21]. The vertical dash-dotted line is located at the coupling streamwise coordinate for both PSE-DNS and PSE-LES.

IV. Results

A. Predicting the point of transition

Predicting the correct point of transition strongly affects many factors of high practical significance such as the distribution of wall-shear stress or surface heat transfer. As a consequence, the accuracy of its computation becomes of foremost importance for reliable estimates of drag and surface temperature.

The skin-friction coefficient C_f is usually considered a good marker for detecting the point where the flow diverges from the laminar solution, and its values are shown in Fig. 3 for the three cases presented in Table 1. In PSE-DNS, the point of transition is accurately predicted despite the strong reduction in the number of degrees of freedom attained in the pre-transitional region (from 100M to 0.2M), consistent with Joslin et al. [10]. The results demonstrate that the PSE faithfully account for the linear and nonlinear growth of disturbances that ultimately result in the breakdown of the laminar flow. This will be further discussed in Section B. The transition point is still correctly captured in PSE-LES, which shows a good skin-friction correlation in both the laminar and turbulent regions even after reducing the total number of grid points by a factor of 100 in the latter (from 150M to 4M).

The above findings are in contrast to the RANS-based approaches, which fail to predict the correct location of the transition even at a considerably higher number of grid points [4]. Moreover, when LES is used in the entire domain, constant coefficient models also fail to differentiate between laminar and turbulent flows, and the turbulent eddy-viscosity remains active throughout the whole domain, inhibiting the growth of perturbations as discussed in Sayadi and Moin [3]. This issue is completely bypassed here by treating the pre-transitional region via PSE. Another added advantage of PSE compared to LES is a reduction of the computational cost by at least an order of magnitude.

The most noteworthy deficiency of PSE-LES compared with DNS-DNS is the faster growth of the friction coefficient in the transitional region, presumably due to the lack of resolution required to capture the full dynamic breakdown of the lambda vortices. Fig. 4 contains the instantaneous wall-normal velocity during the transition for PSE-LES, and should be compared with its DNS-DNS counterpart in Fig. 2. The LES resolution (see Table 1) is fine enough to capture the lambda vortices, although they are noticeably shorter in x. Moreover, the second row in the staggered vortex configuration is lost, which may explain the faster growth observed in C_f. As the breakdown of the lambda vortices was correctly represented in PSE-DNS, the issue is probably related to the performance of the dynamic Smagorinsky model and leaves room for future improvements in subgrid-scale modeling.
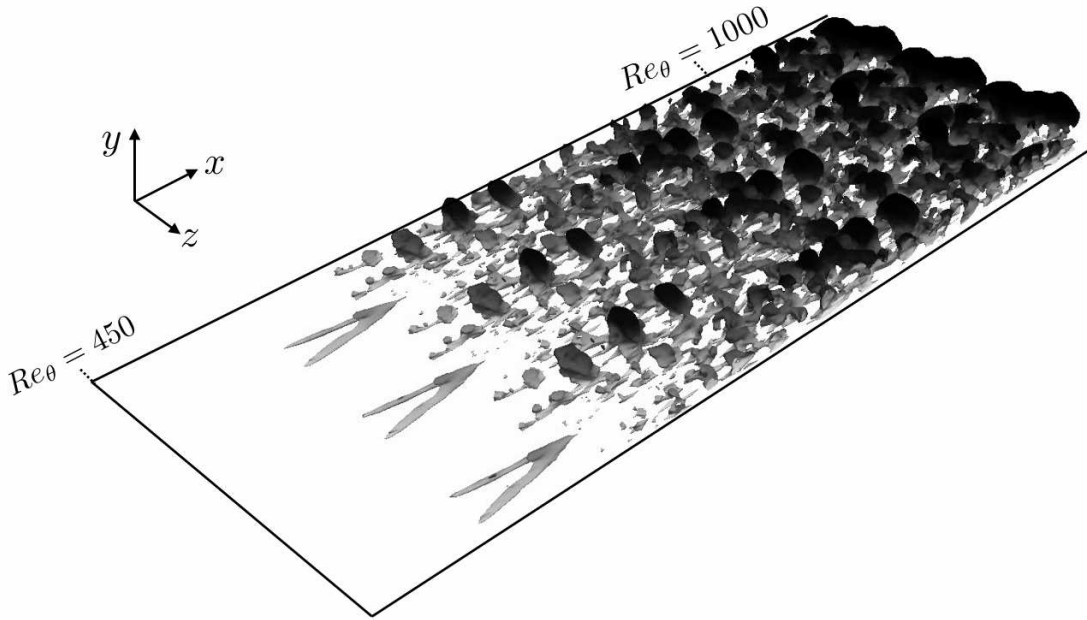
5

Fig. 4   Isocontours of positive instantaneous wall-normal velocity at a value of $3 \times 10^{-2} U_\infty$ for PSE-LES.

B. Pre-transitional region

The skin-friction coefficient discussed above is a low-order statistic with little information about the structural behavior of the flow. In this section we wish to analyze more carefully the differences and similarities between DNS and PSE solutions in the pre-transitional region. For that purpose, we compare the spanwise and temporal Fourier transforms of the streamwise velocity. We focus on the two most representative modes, the fundamental and subharmonic waves defined in Section III as those corresponding to the spanwise and time wavenumber pairs $(0, \omega)$ and $(\beta, \omega/2)$, respectively.

The results are presented in Fig. 5 as a function of the streamwise and wall-normal directions. The agreement is reasonably good and the PSE capture the downstream evolution of the TS wave as well as the exponential growth of the subharmonic mode, in accordance with the accurate prediction of the point of transition discussed in Section A. Although not shown, the resulting transitional lambda vortices from PSE-DNS are visually indistinguishable from those obtained for DNS-DNS plotted in Fig. 2.

While the PSE faithfully capture the evolution of the TS wave and subharmonic modes, a detailed comparison of the maximum root-mean-squared (rms) values of the velocity modes (not shown) reveals differences between the PSE and DNS for some of the harmonics. Nevertheless, the results from Section A suggest that these differences do not play an important role in determining the point of transition or the physical structure of the transitional lambda vortices. Preliminary calculations pointed out that the streamwise matching location between PSE and DNS needs to be far enough from the PSE breakdown point in order to obtain healthy results. This prevents resolving rapid variations of the shape functions in the late stages of the transition, which may violate the key assumption underlying the PSE.

C. Turbulent region

In this last section we evaluate the performance of PSE-LES in the turbulent region right after transition to turbulence. Some test cases not reported here suggest that once the lambda vortices break into a chaotic state, the role of the LES becomes more prominent. This is also supported by previous works on flat-plate boundary-layer transition where different tripping methods converge to the same turbulent state once the upstream conditions are forgotten [22]. It follows that past the breakdown to turbulence, the influence of the PSE solution rapidly diminishes.

Despite the secondary role of PSE in the turbulent region, the analysis is still relevant since both PSE and LES must interact accordingly in the first stages after the transition in order to produce realistic turbulence.
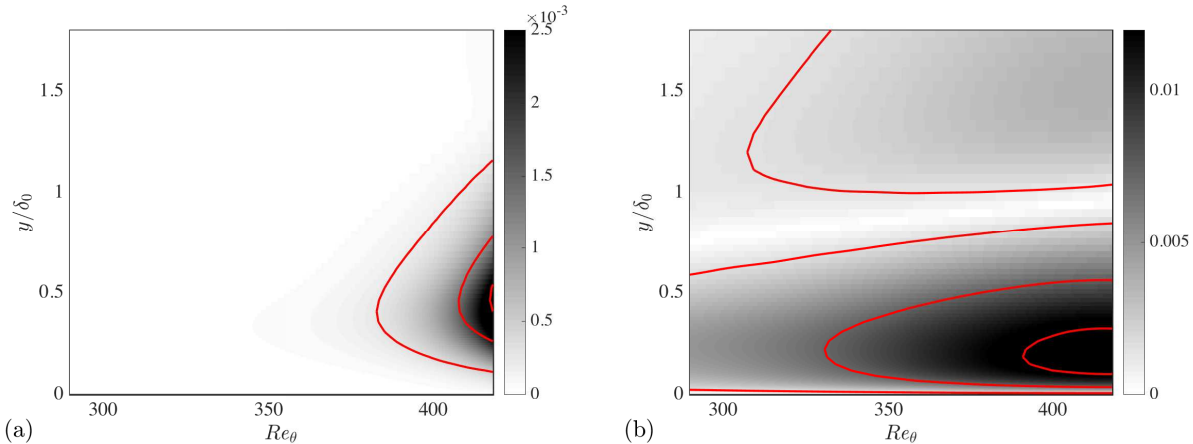
Fig. 5 **Root-mean-squared of the streamwise velocity Fourier modes as a function of Re_θ and wall-normal distance. (a) Subharmonic mode $(\beta, \omega/2)$ and (b) fundamental mode $(0, \omega)$. Colors for the DNS-DNS case. The solid red lines are 0.1, 0.5 and 0.9 of the maximum for the PSE-DNS case.**

Fig. 6 compares the mean streamwise velocity profile and rms fluctuating velocity for the three computations at $Re_\theta = 1000$. Velocities and lengths are scaled in local wall units. The rms velocity exhibits a good agreement. On the other hand, the differences in the mean velocity profile are close to 10% in the wake region, although such an error can be argued to be acceptable given the aggressive reduction in the number of degrees of freedom, which is of the order of 100 times smaller in favor of the PSE-LES approach.

Since U_∞ is imposed as the top boundary condition in both DNS and LES computations, the aforementioned velocity deficit in the LES wake is a direct consequence of wrong viscous stress at the wall, later used to non-dimensionalize the mean velocity in wall units. As discussed in Section A, the issue is unrelated to PSE, which has been shown to perform properly, and future improvements in the turbulent region should focus on enhanced subgrid-scale models and wall-modeled LES.

V. Conclusions

In the present study we have investigated the capabilities of the parabolized stability equations to provide accurate predictions in the zero-pressure-gradient H-type natural transition scenario. A set of three numerical simulations were performed to assess the suitability of the PSE to, first, model the laminar region and, second, act as an inflow inlet condition in DNS and LES just before the onset of transition. The results showed that the PSE-DNS combination is able to provide an accurate representation of the pre-transitional region, including the prediction of transition, growth of the most significant modes, and correct one-point statistics in the turbulent region right after the breakdown, which were shown to be identical to those computed by DNS of the full domain. Further computational savings, of the order of 100 times compared with DNS, were achieved by combining PSE with wall-resolved LES for the transitional and turbulent zones while still reproducing the statistics along the full boundary layer domain with reasonable accuracy.

Acknowledgments

References

[1] Slotnick, J., Khodadoust, A., Alonso, J., Darmofal, D., Gropp, W., Lurie, E., and Mavriplis, D., *CFD Vision 2030 Study: A Path to Revolutionary Computational Aerosciences*, Tech. Rep. CR–2014-218178, NASA, 2014.

[2] Lozano-Durán, A., Hack, M. J. P., and Moin, P., "Modeling boundary-layer transition in direct and large-eddy simulations using parabolized stability equations," *Phys. Rev. Fluids*, Vol. 3, 2018, p. 023901.
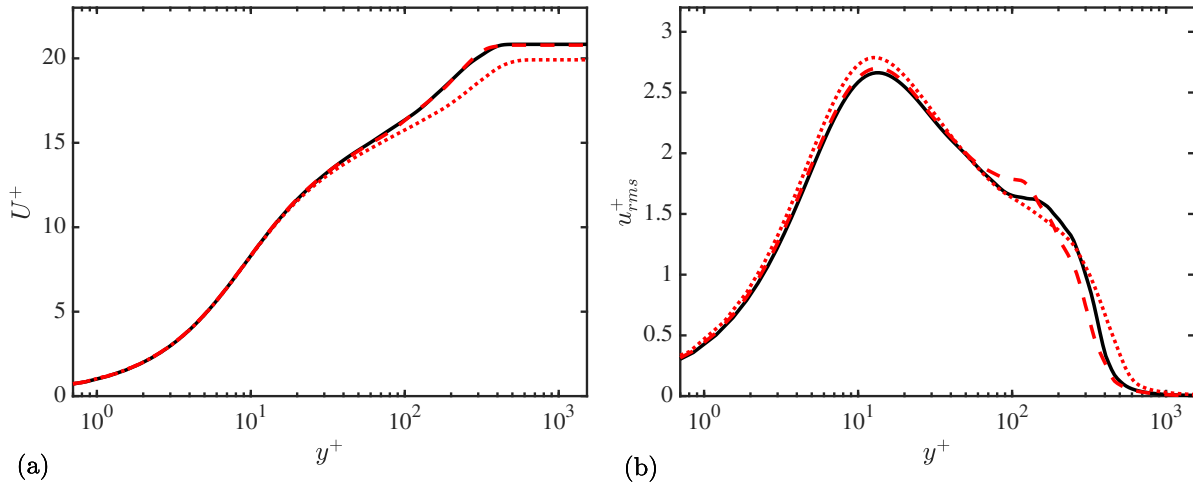
7

Fig. 6 **(a) Mean and (b) root-mean-squared streamwise velocity fluctuations at** Re_θ = 1000. **Solid (black), DNS-DNS; dashed (red), PSE-DNS; dotted (red), PSE-LES.**

[3] Sayadi, T., and Moin, P., "Large eddy simulation of controlled transition to turbulence," *Phys. Fluids.*, Vol. 24, No. 11, 2012, p. 114103.

[4] Pasquale, D., Rona, A., and S.J., G., "A selective review of CFD transition models," 2009.

[5] Herbert, T., "Boundary-layer transition - analysis and prediction revisited," *AIAA Pap.*, Vol. 91, 1991, p. 0737.

[6] Bertolotti, F. P., Herbert, T., and Spalart, P. R., "Linear and nonlinear stability of the Blasius boundary layer," *J. Fluid Mech.*, Vol. 242, 1992, pp. 441–474.

[7] Herbert, T., "Parabolized stability equations," *Annu. Rev. Fluid Mech.*, Vol. 29, 1997, pp. 245–283.

[8] Hack, M. J. P., and Moin, P., "Towards modeling boundary layer transition in large-eddy simulations," *Annual Research Briefs*, 2015, pp. 137–144.

[9] Esfahanian, V., Hejranfar, K., and Sabetghadam, F., "Linear and nonlinear PSE for stability analysis of the Blasius boundary layer using compact scheme," *J. Fluids Eng.*, Vol. 123, 2001, pp. 545–550.

[10] Joslin, R. D., Streett, C. L., and Chang, C.-L., "Spatial direct numerical simulation of boundary-layer transition mechanisms: Validation of PSE theory," *Theor. Comp. Fluid Dyn.*, Vol. 4, No. 6, 1993, pp. 271–288.

[11] Haj-Hariri, H., "Characteristics Analysis of the Parabolized Stability Equations," *Stud. Appl. Math.*, Vol. 92, No. 1, 1994, pp. 41–53.

[12] Day, M. J., Mansour, N. N., and Reynolds, W. C., "Nonlinear stability and structure of compressible reacting mixing layers," *J. Fluid Mech.*, Vol. 446, 2001, pp. 375–408.

[13] Orlandi, P., *Fluid flow phenomena: A numerical toolkit*, 2000, Fluid Mechanics and its Applications, Vol. 55, pp. 1–345.

[14] Wray, A. A., "Minimal-storage time advancement schemes for spectral methods," *NASA–Ames Research Center, Moffett Field, CA*, , No. private communication, 1986.

[15] Kim, J., and Moin, P., "Application of a fractional-step method to incompressible Navier–Stokes methods," *J. Comput. Phys*, Vol. 59, 1985, pp. 308–323.

[16] Germano, M., Piomelli, U., Moin, P., and Cabot, W., "A dynamic subgrid-scale eddy viscosity model," *Phys. Fluids.*, Vol. 3, No. 7, 1991, pp. 1760–1765.

[17] Lilly, D. K., "A proposed modification of the Germano subgrid–scale closure method," *Phys. Fluids.*, Vol. 4, No. 3, 1992, pp. 633–635.

[18] Bae, H. J., Lozano-Durán, A., Bose, S. T., and Moin, P., "Turbulence intensities in large-eddy simulation of wall-bounded flows," *Phys. Rev. Fluids*, Vol. 3, 2018, p. 014610.

[19] Lozano-Durán, A., and Bae, H. J., "Convergence of large-eddy simulation in the outer region of wall-bounded turbulence," *Center for Turbulence Research - Annual Research Briefs*, 2017, pp. 257–270.

[20] Lozano-Durán, A., Bae, H. J., Bose, S. T., and Moin, P., "Dynamic wall models for the slip boundary condition," *Center for Turbulence Research - Annual Research Briefs*, 2017, pp. 229–242.

[21] Sayadi, T., Hamman, C. W., and Moin, P., "Direct numerical simulation of complete H-type and K-type transitions with implications for the dynamics of turbulent boundary layers," *J. Fluid Mech.*, Vol. 724, 2013, pp. 480–509.

[22] Schlatter, P., and Örlü, R., "Turbulent boundary layers at moderate Reynolds numbers: inflow length and tripping effects," *J. Fluid Mech.*, Vol. 710, 2012, pp. 5–34.